Understanding the dynamic contribution to future changes in tropical precipitation from low-level convergence lines

Evan Weller[1,2,3]*, Christian Jakob[1,2], and Michael J. Reeder[1,2]

[1]School of Earth, Atmosphere and Environment, Monash University, Victoria, Australia

[2]Centre of Excellence for Climate System Science, Monash University, Victoria, Australia

[3]School of Environment, The University of Auckland, Auckland, New Zealand

Revised submission to *Geophysical Research Letters* (2019-1-14)

* Corresponding author:

Evan Weller

School of Environment, The University of Auckland, Private Bag 92109, Auckland, 1004, New Zealand.

E-mail: evan.weller@auckland.ac.nz

Key Points

The spatial patterns of future precipitation change, and most of the regional uncertainty, are dominated by the dynamic contributions.

The dynamic contribution to future precipitation change is strongly related to frequency and strength changes of transient convergence lines.

Accurate future precipitation predictions require accurate simulations of short-lived weather systems of which convergence lines are a part.

Abstract

Future precipitation changes include contributions from both thermodynamic and dynamic processes. Given that precipitation in the tropics is commonly associated with convergence lines, we construct a simple linear regression model relating the convergence line frequency and strength to precipitation at sub-daily time-scales, and use it to show that changes in the convergence lines are related to the dynamical change in the precipitation. Given GCM-predicted convergence line changes, we predict precipitation changes using the regression model. The so-predicted precipitation change is equivalent to the dynamical component of the precipitation change identified in earlier studies that used very different methods. The difference between the precipitation change in GCMs and that predicted from changes in convergence lines accounts for thermodynamic and other potentially important dynamical contributions. More accurate predictions of future precipitation therefore require the accurate simulations of the relatively short-lived weather features responsible for convergence lines in the tropics in GCMs.

Plain Language Summary

Future changes in precipitation have been shown to have contributions from both thermodynamic and dynamic processes. Although the thermodynamic part is reasonably well understood (through the Clausius-Clapeyron relationship), the dynamical part is not. Moreover, the spatial pattern of the precipitation change and much of the regional uncertainty in projections of this change, especially in the tropics, are dominated by the dynamic contributions. Therefore, we have investigated the underlying processes for the dynamical part and discovered that changes in the "weather" of atmospheric convergence lines constitute a large part of the dynamic contribution to precipitation changes in a future climate. The implications of this are not only that we now know the main ingredient for change, but also that it is the weather time-scales that we need to simulate well in models for us to predict this important contribution to climate change.

Introduction

Predicting changes in regional precipitation due to greenhouse warming remains an important challenge (e.g., Knutti and Sedláček, 2013). The two main contributors to this change, both to the mean and the extremes, are increases in atmospheric moisture due to warming (the primary thermodynamic contribution to precipitation changes) and changes in the atmospheric circulation (the primary dynamic contribution to precipitation changes) (Allen and Ingram, 2002; Ma and Xie, 2013; O'Gorman, 2015; Pfahl et al., 2017; Tandon et al., 2018; Wills et al., 2016). The dynamical change in the tropical precipitation is mostly consistent with changes in the spatial patterns of the low-level convergence and convection, which are thought to be driven by changes in the sea surface temperature (SST) gradient, land-sea temperature contrast, and the local atmospheric circulation (Chadwick et al., 2013; Huang et al., 2013; Kent et al., 2015; Lambert et al., 2017; Ma and Xie 2013; Xie et al., 2010). Over the oceans, the spatial pattern of the change in the vertical motion also appears to be consistent with the idea that changes in the spatial pattern of SST drive most of the change in the low-level convergence and the location of the convection (Chadwick et al., 2013; Huang et al., 2013; Kent et al., 2015; Xie et al., 2010).

Although changes in the precipitation cannot be separated into thermodynamic and dynamic contributions unambiguously, the idea is useful nonetheless. Several previous studies have devised methods based on the convective mass flux to decompose the precipitation changes predicted by GCMs into their thermodynamics and dynamic contributions (e.g., Chadwick et al., 2013; Kent et al., 2015). Other studies have used the vertically averaged vertical motion to define the dynamic contribution to precipitation change (e.g., Bony et al., 2013; Endo and Kitoh 2014). All of these previous studies have been based on monthly mean data.

Large amounts of precipitation in the tropics (30-60% over land and >65% over oceans) fall in relatively short-lived events associated with convergence lines (Weller et al., 2017a, 2017b). The convergence of mass along these lines is associated with low-level upward motion which commonly triggers convection, although there has been much debate over the decades as to whether convergence should be thought of as a consequence or a cause of (trigger for) convection. It is not the intention of the present study to address this debate and assign causality; instead it is to simply exploit the close relationship between low-level convergence lines and precipitation. Convergence lines can be formed by weather features such as the equatorward extension of fronts, gravity waves, boundary layer rolls, evaporatively-driven cold pools, and topographically generated weather systems such as mountain waves and sea and land breezes (Weller et al., 2017a). However, when averaged over longer time- and space-scales, these short-lived convergence lines form the well-known tropical convergence zones (Berry and Reeder, 2014; Hastenrath, 1995; Widlansky et al., 2013; Wodzicki and Rapp, 2016), such as the Inter-Tropical Convergence Zone (ITCZ) and South-Pacific Convergence Zone (SPCZ) that dominate the larger-scale, longer-term rainfall variability (Borlace et al., 2014; Cai et al., 2012; Vincent et al., 2011; Weller et al., 2014).

Weller et al. (2017b) made the point that changes in convergence lines, at least *qualitatively*, appear to account for the dynamical component of the change in precipitation. The present work builds on Weller et al. (2017b) and addresses *quantitatively* the question as to whether or not convergence lines are the tropical weather systems underpinning the dynamical change in the precipitation. To this end, we develop a simple linear regression model relating the frequency and strength of convergence lines to the precipitation at sub-daily time-scales and show that the model successfully reconstructs the observed precipitation. Then, using climate simulations from the models participating in the Coupled Model Intercomparison Project Phase 5 (CMIP5; Taylor et al., 2012) for the late 21st century, we calculate the future changes in precipitation related solely to changes in the sub-daily convergence line occurrence and strength and compare these changes to the dynamic precipitation changes identified by other methods that use monthly-averaged fields. We then discuss the relationship of the residual precipitation change (the difference between the total and dynamic contribution) to the thermodynamic contribution and other dynamical changes not explained by changes in the convergence lines.

Methods

Observation-based convergence lines and precipitation.

Instantaneous convergence lines were identified objectively in the European Centre for Medium Range Weather Forecasting (ECMWF) reanalysis (ERA-Interim, Dee et al., 2011) using 1.5° horizontal resolution wind fields and applying the method detailed in Weller et al. (2017a). The convergence lines are identified in 6-hourly divergence fields calculated at 850 hPa for the period 1979–2005. In addition, the minimum divergence threshold is set to zero (i.e., all regions of convergence are included), following Weller et al. (2017b). Note, only two points are required by the joining algorithm that is used to link minima points in the divergence fields for a convergence line to be identified (Weller et al., 2017b). However, objectively identified convergence lines are not always geometrically linear when more than two points constitute an identified synoptic feature. The method also identifies geometrically complicated convergence lines. We refer to all identified convergence features as lines only when they are recognized to be a singular feature by the joining algorithm. Note, convergence lines with only two points constitute only a small proportion (~0.1%) of all lines that are identified in the ERA-Interim reanalysis. Further, <15% of all convergence lines identified in ERA-Interim exhibit a length less than the peak (~600km) in their distribution, which has a long tail and 50% of lines are longer than ~1400 km.

Once the convergence lines are identified, they are associated with the National Oceanic and Atmospheric Administration (NOAA)/Climate Prediction Center (CPC) morphing technique (CMORPH, Joyce et al., 2004) 6-hourly accumulated precipitation when a convergence line is found sufficiently close (i.e., adjacent grid points) to the precipitation grid point (see Weller et al. (2017a) for details). It is noted that ERA-Interim winds are often based on relatively few observations over the tropics, and therefore the degree to which they represent reality is uncertain. Similarly, CMORPH has been shown to capture the spatial precipitation distribution patterns well, although it overestimates the precipitation in the tropic to subtropics, underestimates it in the middle to high latitudes, and overestimates (underestimates) weak (strong) intensities (e.g., Joyce and Xie, 2011). However, CMORPH provides higher temporal (sub-daily) resolution compared to other datasets, such as the Global Precipitation Climatology Project (GPCP).

CMIP5 model convergence lines and precipitation.

A total of 10 CMIP5 models (Taylor et al., 2012; see Supplementary Table 1) are used given their availability of the required sub-daily (6-hourly) data (Weller et al., 2017b). Objectively identified convergence lines and the associated precipitation are calculated from current climate (Historical) simulations with anthropogenic forcing (greenhouse gases, aerosols, and other anthropogenic forcing agents) and natural forcing (solar and volcanic activities) for the period

1979–2005, and high emissions future climate (Representative Concentration Pathway 8.5, RCP8.5) simulations for the period 2080–2099. Output from each model is interpolated onto the ERA-Interim 1.5° horizontal grid prior to the calculation of divergence, identifying the convergence lines, and the proportion of precipitation associated with these convergence lines (see Weller et al. (2017b) for extended details of the calculations of convergence lines from models). Although the interpolation of GCM output (or the stage at which it is performed) is not always ideal, Weller et al. (2017b) show that it did not determine the results of their study. For example, there are no clear relationships between the original resolution of a model and the respective bias in the historical simulations (see Supplementary Table 1), nor future changes in the dynamical contribution to precipitation. For all results that show spatial maps, regions with surfaces above 850 hPa are shaded gray as they are not analyzed.

Regression model

We use simple linear regression to estimate the precipitation associated with a convergence line using the equation $PR_{dyn} = a_1 \cdot CLS + b$, where PR_{dyn} is the grid-point precipitation associated with a convergence line, and CLS is the instantaneous grid-point strength of the convergence line (i.e., the strength of the convergence line point closest to the precipitation is assigned to that precipitation point). Using the grid-point relationships found for the observations and the individual CMIP5 models over the odd years (e.g., 1999, 2001, etc.) during the periods 1998–2013 and 1979–2005, respectively (Supplementary Fig. 2 shows maps of the observed and MMEM regression coefficients), we reconstruct the climatological precipitation associated with convergence lines over the even years (e.g., 1998, 2000, etc.) during the same periods. For example, when a convergence line occurs, the precipitation is calculated using the strength of the convergence line, then for each grid-point, the precipitation is averaged over the historical period to generate climatological maps. Here the reconstructed precipitation is used to represent the dynamical component of precipitation. For CMIP5 RCP8.5 simulations, we similarly reconstruct the component of the precipitation associated with convergence lines over the period 2080–2099. However, we use the historical grid-point regression relationship so that atmospheric moisture content changes (i.e. the thermodynamic contribution to total precipitation changes) do not contribute to the reconstruction of the dynamical component of precipitation associated with convergence lines. We discuss the implications of this in following sections. However, the difference between the future total precipitation changes and the reconstructed precipitation changes is taken to represent the thermodynamic contribution and other contributions not explained using convergence lines to future total precipitation changes.

Results

Although varying in detail, climate models reproduce the overall distribution of precipitation over recent decades (Fig. 1a and b) with a spatial correlation of 0.86 and a root mean square difference of 1 mm day^{-1}. Observations show that over much of the globe large fractions of the total precipitation can be associated with a convergence line (Fig. 1c). This is most evident in high precipitation regions (> 5 mm day^{-1}) of the deep tropics, such as the Indo-Pacific warm pool, but also mid-latitude oceanic regions, and even over land regions such as South America, with fractions greater than 90%. Areas in which a large fraction of the precipitation cannot be associated with convergence lines are confined to the subtropics, where the average precipitation is small (i.e., < 1 mm day^{-1}). Although models slightly (around 10%) overestimate the percentage of the precipitation not associated with convergence lines, they reproduce the spatial pattern of the convergence line to precipitation relationship well (Fig. 1d). It is important to note that in the main tropical convergence zones the models associate the majority of the precipitation (> 75%) with convergence lines (Supplementary Fig. S1).

As precipitation in the tropics is frequently associated with a convergence line, we construct a simple linear regression model for both the observations and each GCM relating the convergence line strength, when present, to the associated six-hourly precipitation (see Methods for the model construction and Supplementary Fig. S2 for the distribution of regression coefficient and intercept terms). We then apply the regression model using the occurrence and strength of the convergence lines to both observations and GCMs to estimate the precipitation at each point. The precipitation is estimated for periods different from those used to develop the regression model. We find that the proportion of the precipitation associated with convergence lines can be faithfully reconstructed (Fig. 2a and b) with large errors confined to regions away from the major convergence zones where the mean precipitation is small. The slight overestimation of the reconstructed precipitation (Fig. 2c and 2d) is partly because some convergence lines are dry (Weller et al., 2017a, 2017b). The regions with large overestimations in the models are where the regression coefficients are large compared with those from observations (Supplementary Fig. S2). The inability of the simple regression model to account for these dry convergence lines leads to an overestimation of the reconstructed precipitation. This overestimation is most evident on the eastern flanks of the subtropical highs and northern Africa, where the atmospheric moisture is low and the frequency of dry convergence lines is high. As our focus is on the regions of high-precipitation, where the errors are small, we conclude that the regression model adequately represents the relationship between convergence strengths and precipitation.

Assuming the only change in a future climate is a change in frequency and strength of convergence lines (Fig. 3), the future precipitation can be predicted for each GCM by applying the regression model developed for the current climate to the occurrence and strength changes of convergence lines predicted by each model. In this case the relationship between the convergence strength and the precipitation in the current climate defines the contribution to the precipitation change by the dynamical processes that control convergence line occurrence and strength, but excludes the direct thermodynamic effects of a higher water vapour content in a warmer atmosphere. Note that a possible indirect effect of the increased water vapour in changing the characteristics of convergence lines that form the predictors of the regression model cannot be excluded by this technique.

We first assess the influence of greenhouse warming on changes in the occurrence and strength of convergence lines, by using future greenhouse-gas emission scenarios of RCP8.5, covering the 2080–2099 period (Supplementary Fig. S3). Projections for this future climate period show a general reduction in the frequency and strength of convergence lines over the mid-latitudes consistent with warming-related widening and poleward expansion of subtropical dry zones (Chou et al., 2013; Huang et al., 2013; Lu et al., 2007; Scheff and Frierson, 2012; Seager et al., 2010). In the tropics, large changes in the convergence line frequency are associated with shifts in the major low-latitude convergence zones (Huang et al., 2013; Widlansky et al., 2013).

Using the regression model, we now predict the precipitation change due to changes in convergence line occurrence and strength (Fig. 4b). By construction, this provides a simple yet physically-based representation of a contribution to the dynamical changes hypothesized by other studies (Bony et al., 2013; Chadwick et al., 2013; Endo and Kitoh, 2014; Kent et al., 2015). Importantly, the spatial patterns obtained using our simple prediction strongly resemble those of the previous studies, which are based on completely different techniques. This strong resemblance implies that much of the dynamic contribution to precipitation changes in a warmer climate can be interpreted in terms of changes in the occurrence and strength of low-level convergence lines. Whilst the reasons for these precipitation changes can be manifold, the similarity highlights the importance of synoptic scale dynamical processes. For example, in deep convective situations the strength of the low-level convergence and that of vertical motion at mid-levels are very strongly related. However, the advantage of using the convergence algorithm is that one can search for lines and sub-sample results based on weather feature (i.e., convergence line), rather than grid point properties such as vertical velocities.

Nonetheless there are some notable exceptions. For example, the large increases in the equatorial Pacific in the total precipitation change predicted by the GCMs (Fig. 4a; a modified version of that presented in Fig. 4a of Weller et al. (2017b)) are usually included in previous estimates of the dynamical component of precipitation changes (Bony et al., 2013; Chadwick et al., 2013; Kent et al., 2015; Seager et al., 2010). Our analysis reveals that this large increase in the total precipitation (particularly the western Pacific, indicated by the box in Fig. 4b and 4c) is associated with only a modest increase in convergence line strength (Fig. 3a) and little to no change in frequency (Fig. 3b). Instead, this increase is associated with a relatively large increase in SST (contours in Fig. 4a) and, consequently, atmospheric moisture. Therefore, the difference between the total precipitation changes and the convergence-line-based estimates of precipitation changes (Fig. 4c) is a combination of the thermodynamic contribution and other dynamical contributions that can not be explained using the regression model based on changes in convergence lines alone.

Climate projections show large changes in vertical structure and convective mass-flux in the equatorial Pacific and other regions that are likely to be extremely important to the total precipitation changes (Chadwick et al., 2013; Huang et al., 2013; Seager et al., 2010; Tandon et al., 2018). The difference pattern therefore predominantly highlights the wet-get-wetter, dry-get-drier regions. That is, increases in the moisture convergence in moist, rising branches of the broad circulation, and moisture divergence in the dry, subsidence regions, respectively cause increased and decreased precipitation changes in the future (Bony et al., 2013; Chou et al., 2013; Held and Soden, 2006). It has been suggested that, as the world warms, there will be small changes in the sensitivity of precipitation to convergence (i.e., the slope (a_1) of the regression model as shown in Supplementary Fig. S4a) (e.g., Singh and O'Gorman, 2013; Byrne and O'Gorman, 2016). However, we cannot simply construct the regression model based on the future relationships as it will automatically, by convention, include large contributions due to thermodynamic changes (i.e., changes in the intercept (b) of the regression model as shown in Supplementary Fig. S4b). Such convergence-related signals would also inherently be included in the difference pattern.

Discussion and Conclusion

Changes to the SST pattern are likely to drive shifts in the position of the mean low-level convergence and convection (Ma and Xie, 2013; Windlansky et al., 2013; Xie et al., 2010). This appears to be the case over the equatorial Pacific where changes in the reconstructed precipitation show the off-equatorial convergence zones shifting closer to equator. In the equatorial western Pacific, there is only a small increase in the precipitation associated with changes in the convergence lines; and this increase is more connected to increases in the strength of the convergence lines than increases in their occurrence (*c.f.* Fig. 3 and 4). In the tropical Indian Ocean (indicated by the box in Fig. 3 and 4), an overall decrease in the total precipitation is linked to decreases in both the convergence line occurrence and strength that outweighs an increase from thermodynamic contributions. Generally, regions showing decreases in the total precipitation are characterized by a decrease in the convergence line frequency and/or strength. The reduction of the convergence line strength is particularly marked in the mid-latitudes and is likely to be the result of weaker meridional temperature gradients in a future climate.

Transient low-level convergence lines, defined here using an objectively based line identification technique, are highly important dynamical features associated with precipitation in the current climate. Using vertical motion or any other scalar field such as convergence, tells us little about the synoptic-scale phenomena organizing the precipitation. Imposing geometry on the diagnosis adds information on the synoptics, which is rarely done in tropical meteorology, but is central to mid-latitude meteorology. Overall, we show that the dynamic contribution to the precipitation change in a warmer world as identified in earlier studies can almost entirely be accounted for by changes in the convergence lines. This result reveals a key physical mechanism associated with the change in the precipitation, and highlights that an accurate representation of the weather in climate models, as expressed by the modeled convergence lines, is essential for reliable predictions of the future behaviour of the Earth's climate.

References

Allen, M. R., and W. J. Ingram (2002), Constraints on future changes in climate and the hydrological cycle, *Nature*, 419, 224–232.

Berry, G., and M. J. Reeder (2014), Objective identification of the Intertropical Convergence Zone: Climatology and trends from the ERA-Interim, *J. Clim.*, 27, 1894–1909.

Bony, S. et al. (2013), Robust direct effect of carbon dioxide on tropical circulation and regional precipitation, *Nature Geosci.*, 6, 447–451.

Borlace, S., A. Santoso, W. Cai, and M. Collins (2014), Extreme swings of the South Pacific Convergence Zone and the different types of El Niño events, *Geophys. Res. Lett*., 41, 4695–4703.

Byrne, M. P. and P. A. Gorman (2016), Understanding decreases in land relative humidity with global warming: Conceptual model and GCM simulations, *J. Clim.*, 29, 9045–9061.

Cai, W. et al. (2012), More extreme swings of the South Pacific convergence zone due to greenhouse warming, *Nature*, 488, 365–369.

Chadwick, R., I., Boutle, and G. Martin (2013), Spatial patterns of precipitation change in CMIP5: Why the rich do not get richer in the tropics, *J. Clim.*, 26, 3803–3822.

Chou, C. et al. (2013), Increase in the range between wet and dry season precipitation, *Nat. Geosci*., 6, 263–267.

Dee, D. P. et al. (2011), The ERA-Interim reanalysis: Configuration and performance of the data assimilation system, *Q. J. R. Meteorol. Soc*., 137, 553–597.

Endo, H., and A. Kitoh (2014), Thermodynamic and dynamic effects on regional monsoon rainfall changes in a warmer climate, *Geophys. Res. Lett*., 41, 1704–1710.

Hastenrath, S. (1995), *Climate Dynamics of the Tropics*, 488 pp., Kluwer Acad., Norwell, Mass.

Huang, P., S.-P. Xie, K. Hu, G. Huang, and R. Huang (2013), Patterns of the seasonal response of tropical rainfall to global warming, *Nat. Geosci*., 6, 357–361.

Joyce, R. J., J. E. Janowiak, P. A. Arkin, and P. Xie (2004), CMORPH: A method that produces global precipitation estimates from passive microwave and infrared data at high spatial and temporal resolution, *J. Hydrometeor.*, 5, 487–503.

Joyce, R. J. and P. Xie (2011), Kalman filter-based CMORPH. *J. Hydrometeor.*, 12, 1547–1563.

Kent, C., R. Chadwick, and D. P. Rowell (2015), Understanding uncertainties in future projections of seasonal tropical precipitation, *J. Clim*., 28, 4390–4413.

Knutti, R. and J. Sedláček (2013), Robustness and uncertainties in the new CMIP5 climate model projections, *Nat. Clim. Change,* 3, 369–373.

Lambert, F. H., A. J. Ferraro, and R. Chadwick (2017), Land–ocean shifts in tropical precipitation linked to surface temperature and humidity change, *J. Clim.,* 30, 4527–4545.

Lu, J., G. A. Vecchi, and T. Reichler (2007), Expansion of the Hadley cell under global warming, *Geophys. Res. Lett*., 34, L06805.

Ma, J., and S.-P. Xie (2013), Regional patterns of sea surface temperature change: A source of uncertainty in future projections of precipitation and atmospheric circulation, *J. Clim*., 26, 2482–2501.

O'Gorman, P. A. (2015), Precipitation extremes under climate change, *Curr. Clim. Change Rep.*, 1, 49–59.

Pfahl, S., P. A. O'Gorman, and E. M. Fischer (2017), Understanding the regional pattern of projected future changes in extreme precipitation, *Nature Clim. Change*, 7, 423–427.

Scheff, J. and D. Frierson (2012), Twenty-first-century multimodel subtropical precipitation declines are mostly midlatitude shifts, *J. Clim.*, 25, 4330–4347.

Seager, R., N. Naik, and G. A. Vecchi (2010), Thermodynamic and dynamic mechanisms for large-scale changes in the hydrological cycle in response to global warming, *J. Clim*., 23, 4651–4668.

Singh, M. S. and P. A. Gorman (2013), Influence of entrainment on the thermal stratification in simulations of radiative-convective equilibrium, *Geopphys. Res. Lett.*, 40, 4398–4403.

Tandon, N. F., X. Zhang, and A. H. Sobel (2018), Understanding the dynamics of future changes in extreme precipitation intensity, *Geophys. Res. Lett*., 45, 2870–2878.

Taylor, K. E., R. J. Stouffer, and G. A. Meehl (2012), An overview of CMIP5 and the experiment design, *Bull. Amer. Meteor. Soc.,* 93, 485–98.

Vincent, E. M. et al. (2011), Interannual variability of the South Pacific Convergence Zone and implications for tropical cyclone genesis, *Clim. Dynam*., 36**,** 1881–1896.

Weller, E. et al. (2014), More-frequent extreme northward shifts of eastern Indian Ocean tropical convergence under greenhouse warming, *Sci. Rep.,* 4, 6087.

Weller, E., K. Shelton, M. J. Reeder, and C. Jakob (2017a), Precipitation associated with convergence lines, *J. Clim*., 30, 3169–3183.

Weller, E., C. Jakob, and M. J. Reeder (2017b), Projected response of low-level convergence and associated precipitation under greenhouse warming, *Geophys. Res. Lett*., 44, 10682–10690.

Widlansky, M. J. et al. (2013), Changes in South Pacific rainfall bands in a warming climate, *Nature Clim. Change,* 3, 417–423.

Wills, R. C., M. P. Byrne, and T. Schneider (2016), Thermodynamic and dynamical controls on changes in the zonally anomalous hydrological cycle, *Geophys. Res. Lett.*, 43(9), 4640–4649.

Wodzicki, K. R., and A. D. Rapp (2016), Long-term characterization of the Pacific ITCZ using TRMM, GPCP, and ERA-Interim, *J. Geophys. Res*. *Atmos*., 121, 3153–3170.

Xie, S.-P. et al. (2010), Global warming pattern formation: Sea surface temperature and rainfall, *J. Clim.*, *23*, 966–986.

Acknowledgements

We thank two anonymous reviewers for their constructive comments that led to the improvement of the manuscript. This study was supported by the Australian Research Council Centre of Excellence for Climate System Science (CE110001028). We acknowledge the World Climate Research Programme's Working Group on Coupled Modelling, which is responsible for CMIP, and we thank the climate modelling groups for producing and making their model output available. The ERA-Interim data used here can be obtained via the ECMWF Public Datasets web interface (http://apps.ecmwf.int/datasets/), and CMIP5 data can be obtained via the Earth System Grid data portal (https://cmip.llnl.gov/cmip5/data_portal.html). The convergence line identification code used in the study was that published by Weller et al. (2017a). This research was undertaken with the assistance of resources and services from the National Computational Infrastructure (NCI), which is supported by the Australian Government.

Author Contributions

All authors conceived the study and directed the analysis. E.W. performed the convergence line identification and output analysis. All authors contributed to the initial draft of the paper, interpreting results, discussion of the associated dynamics and improvement of this paper.

Additional Information

Correspondence and requests for materials should be addressed to E.W.

Competing financial interests

The authors declare no competing financial interests.

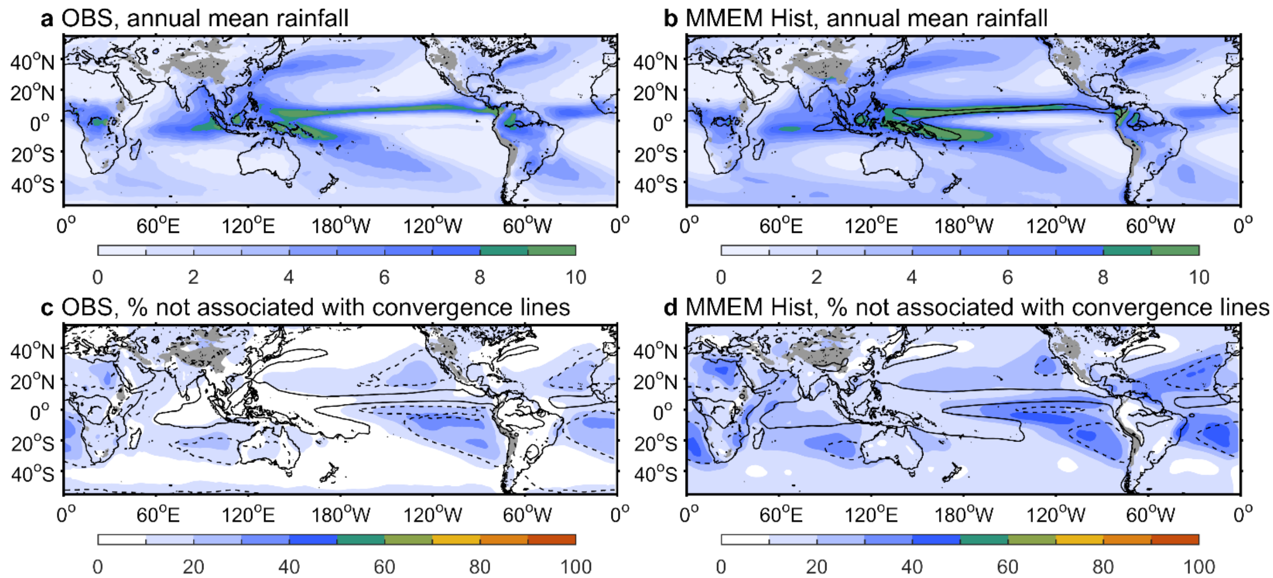

Figure 1 | Comparison of observed and modelled historical climatological precipitation and the proportion not associated with convergence lines. a,**b**, Annual mean total precipitation (in units of mm day^{-1}) from observations and the CMIP5 multi-model ensemble mean (MMEM). The black contour in **b** indicates regions where the observed precipitation is greater than 8 mm day^{-1}. **c**,**d**, Proportion (in units of %) of the total precipitation shown in **a** and **b**, respectively, that does not occur in the presence of convergence lines. In **c** and **d,** the dashed and solid black contours, respectively, indicate regions where the annual mean precipitation is less than 1 mm day^{-1} and greater than 5 mm day^{-1}.

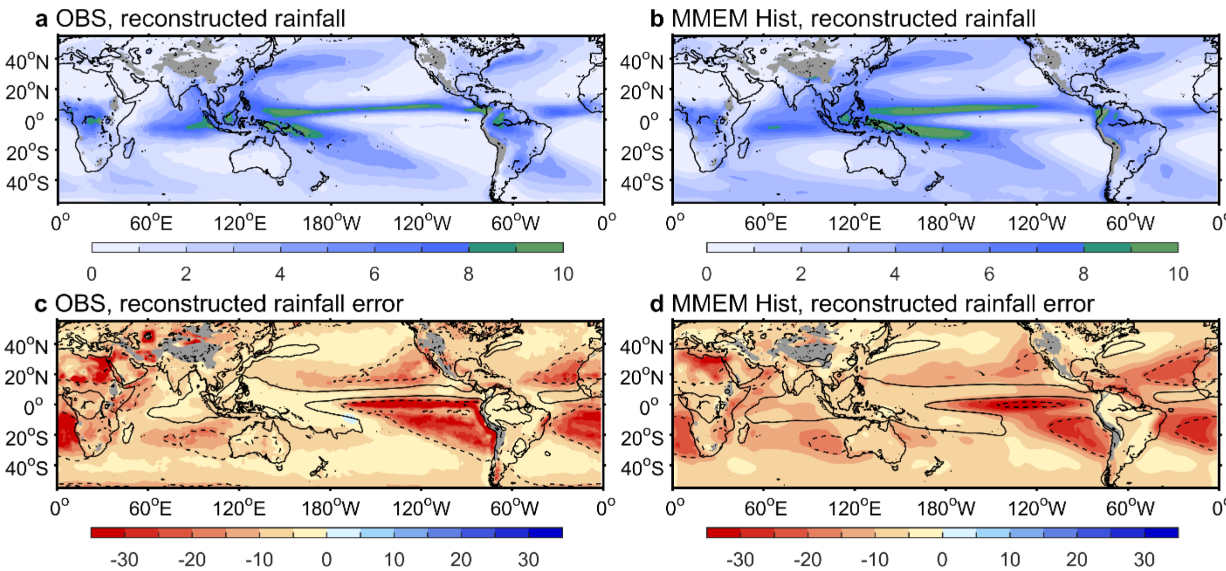

Figure 2 | Reconstruction of the observed and modelled historical precipitation associated with convergence lines. a,**b**, Annual mean precipitation (in units of mm day^{-1}) estimated via a reconstruction using convergence line frequency and strength in linear regression models from observations and the CMIP5 multi-model ensemble mean (MMEM). **c**,**d**, Differences between the amount of precipitation that occurs in the presence of convergence lines and the reconstructed precipitation (in units of %) from observations and MMEM. In **c** and **d,** the dashed and solid black contours, respectively, indicate regions where the annual mean precipitation is less than 1 mm day^{-1} and greater than 5 mm day^{-1}. Red shading indicates an over-estimation of the reconstructed precipitation.

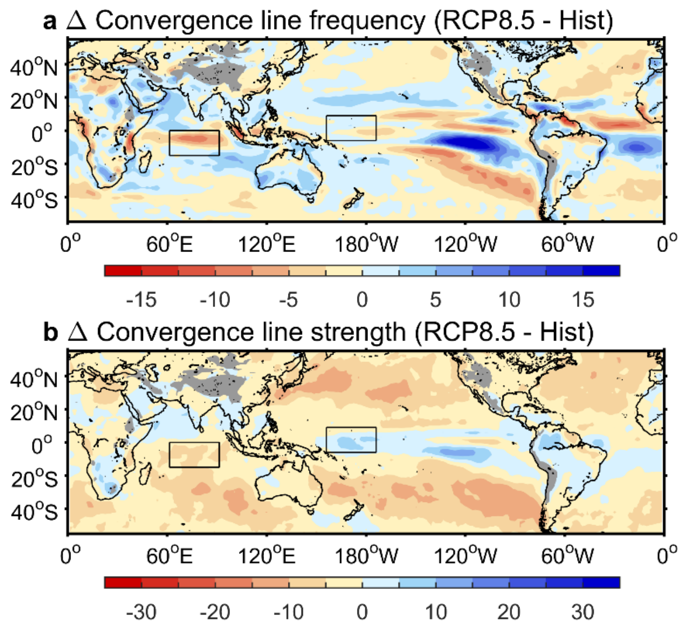

Figure 3 | Future changes in modelled convergence line frequency and strength. a,**b**, The CMIP5 multi-model ensemble mean (MMEM) changes (RCP8.5 2080–2100 minus Historical 1979–2005) in convergence line frequency and convergence line strength (in % of the Historical climatology). The boxes in both panels indicate the western tropical Pacific Ocean and central tropical Indian Ocean regions referred to in the text.

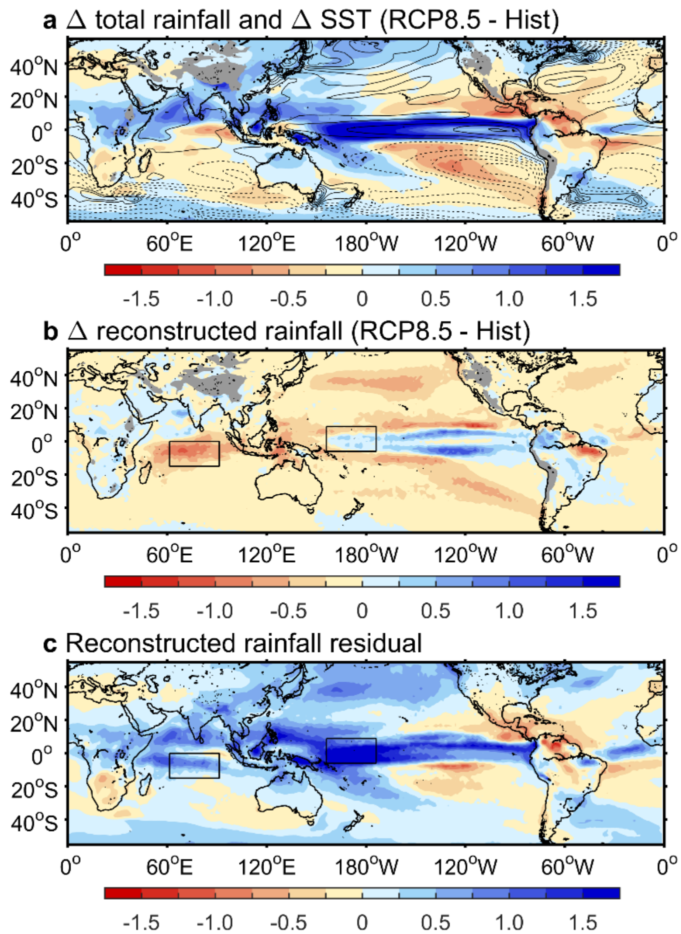

Figure 4 | Future changes in modelled climatological precipitation and its decomposition. a, The CMIP5 multi-model ensemble mean (MMEM) changes (RCP8.5 2080–2100 minus Historical 1979–2005) in annual mean total precipitation (shading) and SST (contours, relative to the tropical (20°S–20°N) mean warming; in units of °C). Blue or red shading indicate increased or decreased precipitation and solid or dashed contours indicate larger or smaller SST warming relative to the tropical mean warming, at intervals of0.25°C. **b**, The MMEM change in annual mean precipitation estimated via the reconstruction using future changes of convergence line frequency and strength, but applying the current climate linear relationship between convergence line strength and precipitation. **c**, The MMEM difference between the change in total precipitation in **a**, and the change in the reconstructed precipitation in **b**. All color scales indicate precipitation changes in units of mm day^{-1}.

Figure 1.

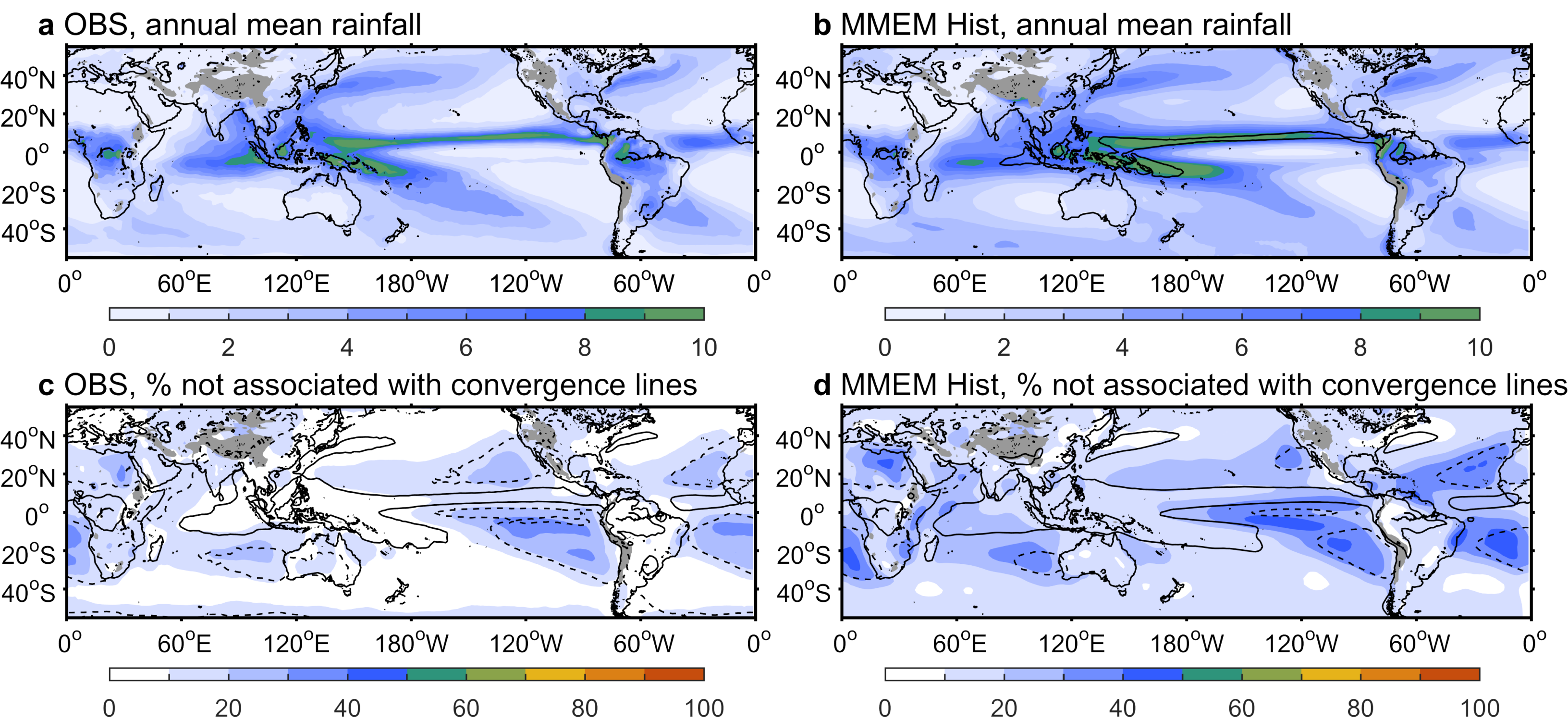
a OBS, annual mean rainfall
b MMEM Hist, annual mean rainfall
c OBS, % not associated with convergence lines
d MMEM Hist, % not associated with convergence lines
40°N
20°N
0°
20°S
40°S
0°
60°E
120°E
180°W
120°W
60°W
0
2
4
6
8
10
0
20
40
60
80
100

Figure 2.

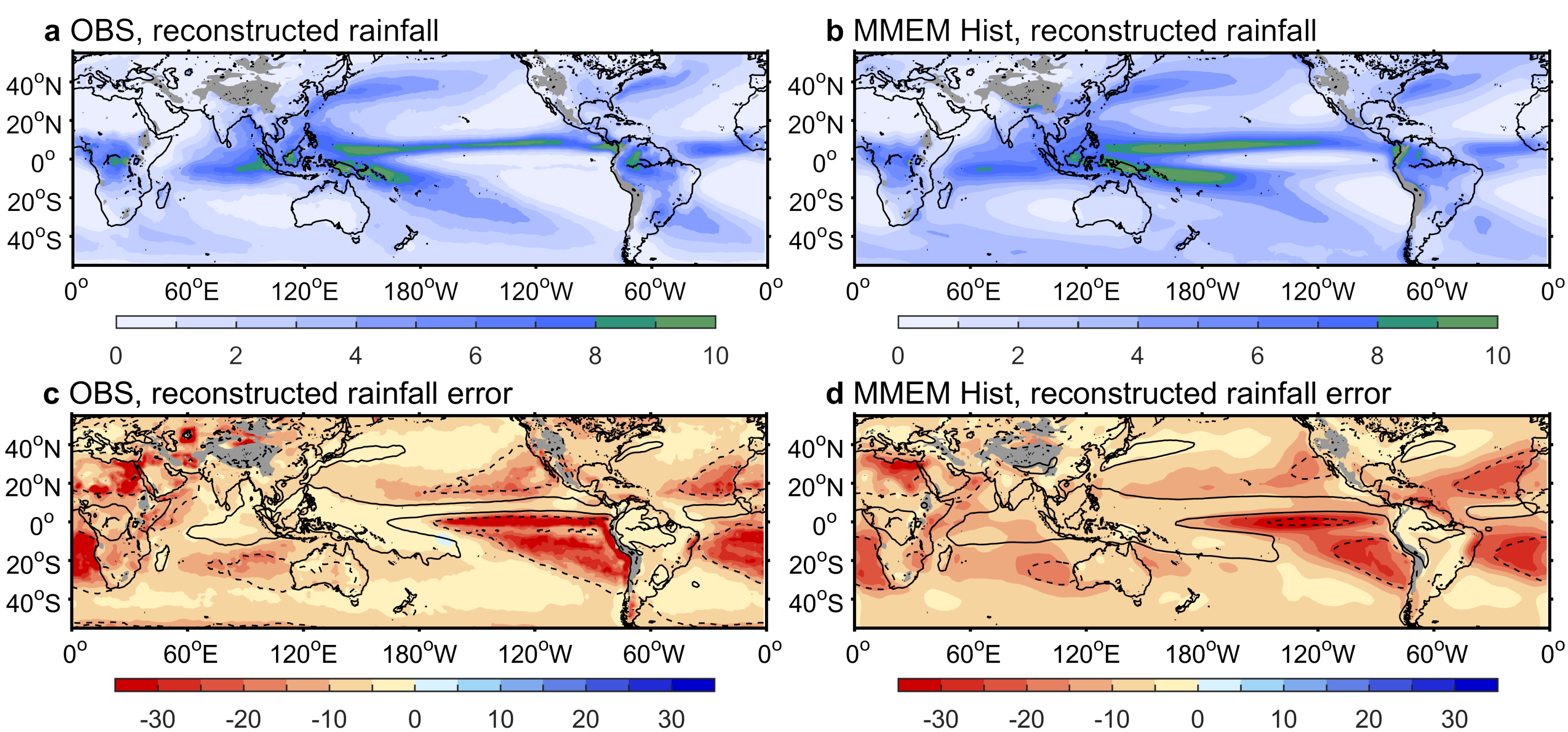
a OBS, reconstructed rainfall
b MMEM Hist, reconstructed rainfall
c OBS, reconstructed rainfall error
d MMEM Hist, reconstructed rainfall error
40°N
20°N
0°
20°S
40°S
0°
60°E
120°E
180°W
120°W
60°W
0
2
4
6
8
10
-30
-20
-10
0
10
20
30

Figure 3.

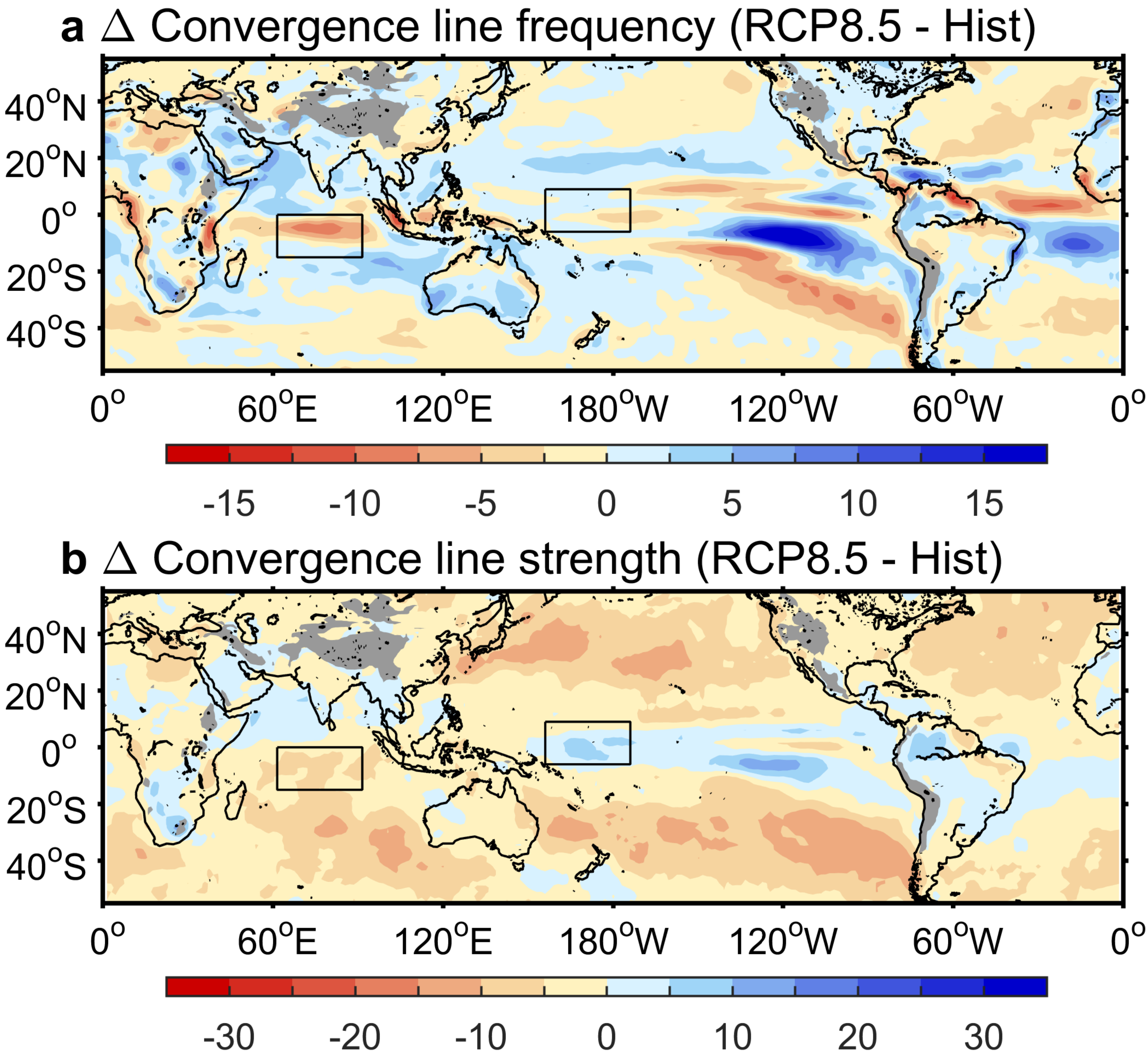
a Δ Convergence line frequency (RCP8.5 - Hist)
40°N
20°N
0°
20°S
40°S
0°
60°E
120°E
180°W
120°W
60°W
0°
-15
-10
-5
0
5
10
15
b Δ Convergence line strength (RCP8.5 - Hist)
40°N
20°N
0°
20°S
40°S
0°
60°E
120°E
180°W
120°W
60°W
0°
-30
-20
-10
0
10
20
30

Figure 4.

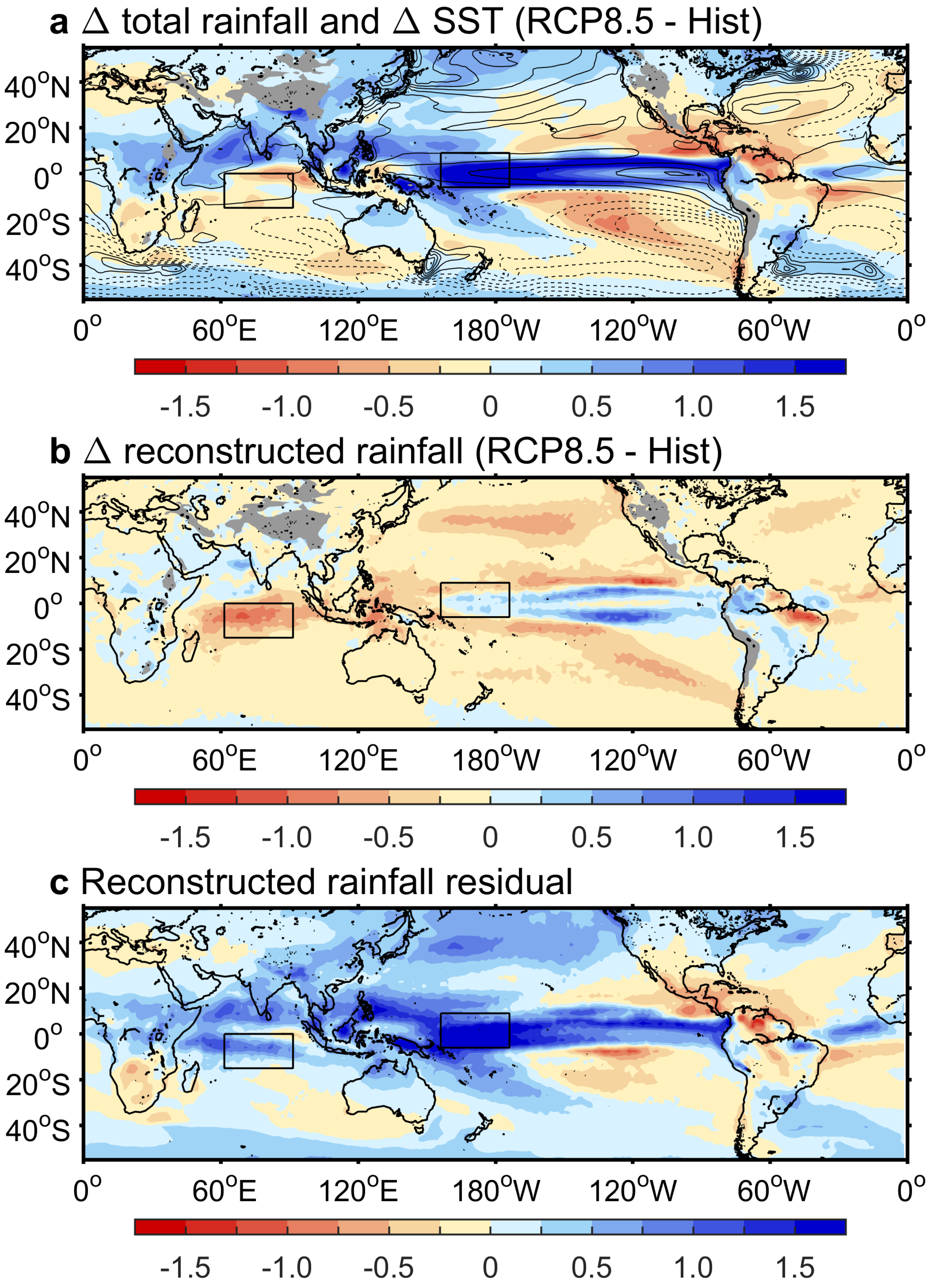
a Δ total rainfall and Δ SST (RCP8.5 - Hist)
b Δ reconstructed rainfall (RCP8.5 - Hist)
c Reconstructed rainfall residual
40°N
20°N
0°
20°S
40°S
0°
60°E
120°E
180°W
120°W
60°W
0°
-1.5
-1.0
-0.5
0
0.5
1.0
1.5